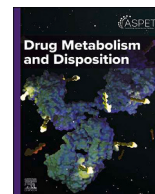




Drug Metabolism and Disposition

journal homepage: www.dmd.aspetjournals.org



SPECIAL SECTION: UTILITY OF MICROPHYSIOLOGICAL SYSTEMS IN PRECLINICAL DRUG DEVELOPMENT—ARTICLE

A primary human Gut/Liver microphysiological system to estimate human oral bioavailability



Yassen Abbas^{1,*} , Morné van Wyk¹ , Hailey Sze¹, James Christophi¹, Ashley A. Spreen², Robert Jarrett Bliton² , Elizabeth M. Boazak² , Tomasz Kostrzewski¹ 

¹ CN Bio Innovations Ltd, Cambridge, United Kingdom

² Altis Biosystems, Durham, North Carolina

ARTICLE INFO

Article history:

Received 5 June 2025

Accepted 15 July 2025

Available online 23 July 2025

Key words:

Bioavailability

Gut liver microphysiological system

Mechanistic modeling

Microphysiological system

Organ-on-a-chip

ABSTRACT

Oral bioavailability is a crucial pharmacokinetic (PK) parameter optimized by drug developers working on new therapeutic compounds. The goal is to obtain adequate systemic exposure and to establish safe and effective therapeutic dosages. Critical to optimizing oral bioavailability is understanding a compound's susceptibility to first-pass metabolism, determined by the intricate relationship between gut absorption, metabolism, and hepatic metabolism. Efforts to model this relationship in vitro have led to the emergence of microphysiological systems (MPSs) that consist of multiple, fluidically linked organs. Here, we describe an MPS that links the gut and liver, capable of simulating both oral and intravenous dosing routes and is made up of entirely primary human cells: a gut barrier tissue comprised of an intestinal epithelial monolayer derived from the human jejunum, and a liver microtissue, derived from primary human hepatocytes. Functionality of gut and liver tissues is maintained in coculture enabling the PK investigation of oral compounds. We combine the primary Gut/Liver MPS with a mechanistic mathematical model to generate organ-specific PK parameters and estimate human oral bioavailability and its components: the fraction absorbed (F_a), the fraction escaping gut wall elimination (F_g), and the fraction escaping hepatic elimination (F_h). We used the CYP3A-mediated compound midazolam, which is subjected to both intestinal and hepatic extraction, to demonstrate the transformative potential of the primary Gut/Liver MPS to mechanistically model the PKs of oral compounds in vitro.

Significance Statement: Bioavailability underpins the success or when insufficient, can stall the development of oral therapeutics. The drug discovery process lacks in vitro assays that can profile the contribution to bioavailability by the gut and liver. The primary Gut/Liver MPS outlined in this study bridges this gap.

© 2025 The Authors. Published by Elsevier Inc. on behalf of American Society for Pharmacology and Experimental Therapeutics. This is an open access article under the CC BY-NC-ND license (<http://creativecommons.org/licenses/by-nc-nd/4.0/>).

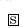
1. Introduction

A central pillar in the development of a new oral medication is to understand its bioavailability, defined as the fraction of drug reaching systemic circulation following absorption in the gut and first-pass metabolism in the liver.¹ The bioavailability of a

compound is affected by both chemical and biological factors, which include solubility/dissolution, permeability, liver clearance, and gastrointestinal metabolism.² Insufficient oral bioavailability has prompted drug developers to either discontinue development, pursue optimization strategies to minimize hepatic and intestinal metabolism, or enhance absorption through the intestinal mucosa.³ Predicting the intricate relationship between gut absorption, metabolism, and hepatic metabolism is critical for optimizing drug bioavailability.⁴

Traditionally, animal models have dominated the prediction of bioavailability, but it is now established that, although animals

* Address correspondence to: Dr Yassen Abbas, CN Bio Innovations Ltd, 332 Cambridge Science Park, Cambridge, UK. E-mail: yassen.abbas@cn-bio.com

 This article has supplemental material available at dmd.aspetjournals.org.

Y.A. and M.vW. contributed equally to this work as first authors.

may be useful qualitative predictors of human bioavailability (ie, low vs high), they are poor quantitative predictors. In a seminal study of 184 compounds, there was no absolute correlation between human and any individual species, or all species taken together, with an R^2 of ~0.34.⁵ This limitation has resulted in the development of in vitro approaches, which aim to dissect the components of oral bioavailability ($F = F_a \times F_g \times F_h$, where F_a is the fraction absorbed, F_g is the fraction escaping gut wall elimination, and F_h is the fraction escaping hepatic elimination).⁶ However, these in vitro methods and this approach to determine bioavailability face significant challenges. For modeling the gut, Caco-2, an immortalized human colorectal adenocarcinoma cell line, is widely used for determining F_a but is limited by its low transporter activity, hindering the study of transported-mediated compounds, and its deficiency in key drug-metabolizing enzymes.⁷ It is now understood that the gut plays a crucial role in drug metabolism, particularly for compounds metabolized by CYP3A, the most abundant and clinically significant group of cytochrome P450 isoenzymes.^{8,9} The limited expression of CYP3A by Caco-2 cells hinders accurate prediction of F_g . Although intestinal microsomes offer an alternative with functional CYP activity, their use is complicated by difficulties in reproducible preparations, the absence of a cell barrier, and the inherent complications associated with heterogeneity of the small intestine compared with the liver.¹⁰ Similarly, for hepatic metabolism, although liver microsomes and suspension hepatocytes are established models, they lack long-term functional enzyme activity.¹¹ Critically, the current in vitro assays assess these processes in isolation. A more integrated in vitro approach is needed, one that combines gut absorption, metabolism, and hepatic metabolism to provide more predictive bioavailability estimations. This work aimed to develop a solution using microphysiological systems (MPSs).

MPS, also known as organ-on-a-chip, are advanced in vitro platforms designed to mimic the complexity and functionality of human organs and tissues. These systems commonly include fluid flow to mimic blood circulation, 3-dimensional (3D) scaffolds to culture cells, and multiple cell types or tissues.^{12,13} By better maintaining the physiological relevance and metabolic function of cells and tissues compared with traditional 2-dimensional cultures, MPSs offer a promising approach for generating more human-relevant absorption, distribution, metabolism, and excretion (ADME) data and improving the in vitro to in vivo translation of drug efficacy and safety data.¹⁴ This has led to the development of multiorgan MPSs that are linked via fluidic connections to better mimic the ADME process of oral compounds.¹⁵ For oral bioavailability studies, linking the gut and liver, and simulating both oral and intravenous (IV) dosing routes, is crucial for in vitro estimation of this key pharmacokinetic (PK) parameter. Although previous Gut/Liver MPSs have been developed and integrated with mechanistic mathematical models to analyze concentration-time data, enabling estimations of parameters such as intrinsic clearance and permeability, a significant limitation remains: the use of immortalized cell lines to model the gut, which often lack sufficient metabolic functionality.^{16,17}

In this work, we addressed this gap by developing a fluidically coupled Gut/Liver MPS entirely derived from primary human tissue. Our primary Gut/Liver MPS consists of 2 compartments containing a gut barrier tissue comprised of an intestinal epithelial monolayer derived from the human jejunum, and a liver microtissue, derived from primary human hepatocytes (PHHs). We combined this dual-organ MPS together with a mechanistic mathematical model to provide an estimate of ADME parameters and oral bioavailability using the CYP3A4-mediated compound, midazolam (MDZ), as a case study.

2. Materials and methods

2.1. Set-up of the Liver MPS

Liver microtissues were established by seeding PHHs (LifeNet Health) on a collagen-coated scaffold in the liver compartment of the Multi-chip Liver-12 plate at a density of 0.6×10^6 viable cells per well. The Liver MPS was cultured using the PhysioMimix Multi-organ System (CN Bio Innovations). Each well of the Liver-12 plate contained a final volume of 1.6 mL of medium and was maintained under a flow rate of $1.0 \mu\text{L/s}$. Cells were seeded in a proprietary Liver Plating Medium (CN Bio Innovations) and cultured under downward flow for 8 hours, then upward flow for 16 hours. At 24 hours, the medium was changed to a proprietary Liver Maintenance Medium (CN Bio Innovations). PHH cell health was evaluated by quantifying the production of lactate dehydrogenase (LDH, Promega's colorimetric assay), and PHH functionality was evaluated by quantifying production of albumin (Albumin ELISA Kit; AssayPro), urea (QuantiChrom Urea assay Kit; Universal Biologicals), and the activity of the CYP3A4 enzyme (CYP3A4 P450-GLO; Promega).

2.2. Set-up of the Gut/Liver MPS

The Gut/Liver MPS integrates a gut barrier tissue with a 3D liver microtissue derived from PHHs. Two types of gut barrier tissues were used: 1 primary, derived from human jejunum stem/progenitor cells (RepliGut—Planar Jejunum; Altis Biosystems, catalog no.: RGP-JEJ-PMX), and the other, a cancer cell line (Caco-2; Public Health England, catalog no.: 09042001), which is considered the current “gold standard” for assessing oral drug absorption. This MPS, referred to as either the primary Gut/Liver MPS or Caco-2/Liver MPS, was cultured using the PhysioMimix Multi-organ System and Multi-chip Dual-organ Consumable Plate (Fig. 1A, CN Bio Innovations). The Dual-organ plate features 6 wells, each containing 2 compartments: 1 for the gut and 1 for the liver. Cell culture media were recirculated by pneumatically driven micro-pumps, allowing independent control of fluid flow in each compartment and the interconnecting channel between the compartments.

2.3. Primary gut model

To establish the primary Gut/Liver MPS, the primary gut tissue was first cultured by expanding the RepliGut Jejunum stem/progenitor cells on 24-well plate (24-WP) Transwells (6.5 mm diameter, $0.4 \mu\text{m}$ pore polyester membrane; Corning) coated with a proprietary hydrogel in RepliGut Growth Medium (RGM, catalog no.: MED-RGM; Altis Biosystems). Medium volumes were $250 \mu\text{L}$ (apical) and $750 \mu\text{L}$ (basal). Eight days postseeding, once the cells reached confluence, the medium was switched to RepliGut Maturation Medium (RMM, catalog no.: MED-RMM; Altis Biosystems) to promote cellular differentiation and polarization. RGM or RMM were changed every 2 days, and gut barrier integrity was assessed using transepithelial electrical resistance (TEER) measurements using an Epithelial Volt/Ohm Meter (EVOM3; World Precision Instruments) and STX2 electrode (World Precision Instruments) daily or every 2 days prior to each medium change after day 10 in culture. The corrected TEER was determined by subtracting the blank Transwell (without cells in RGM or RMM) from the test Transwell and multiplying by the culture surface area.

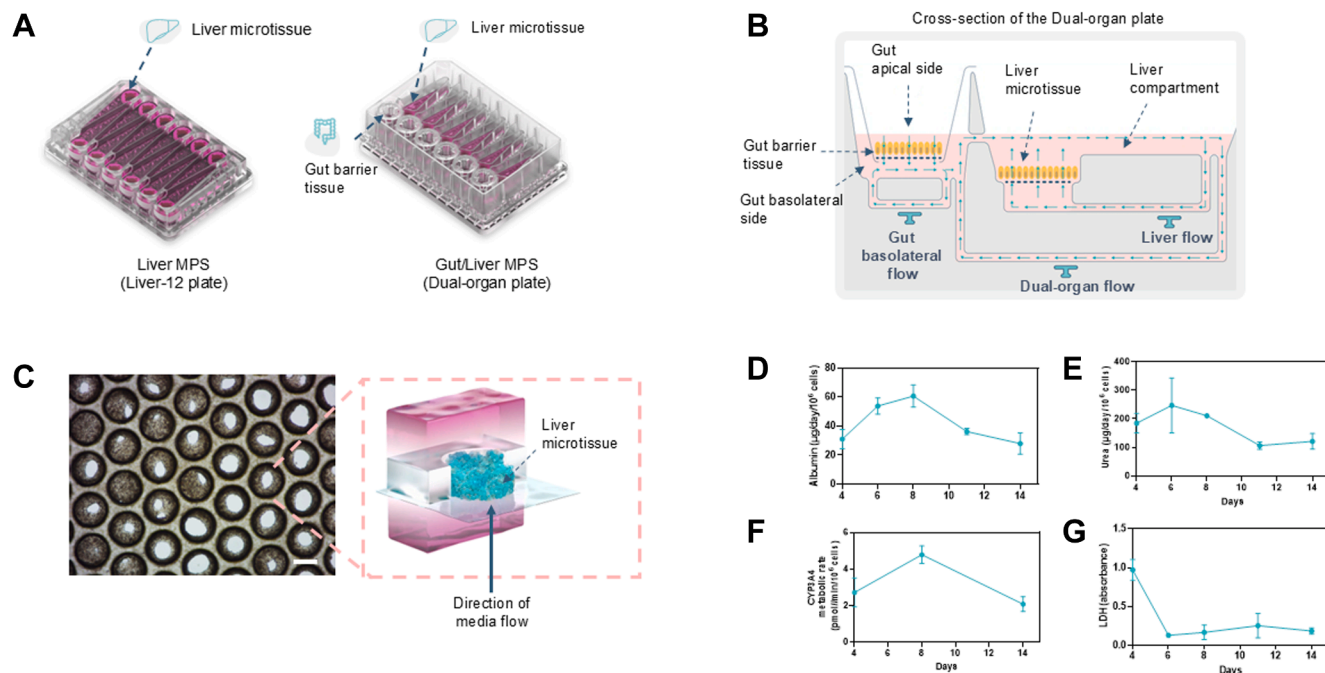


Fig. 1. Establishment of the Liver and Gut/Liver MPS. The Liver MPS and Gut/Liver MPS were cultured using the (A) Liver-12 and Dual-organ plates respectively. (B) Schematic representation of fluid flow within the liver compartment, gut basolateral compartment and the interconnecting channel connecting the compartments, in the Dual-organ plate. Formation of liver microtissue in collagen-coated scaffolds at day 14 of culture by (C) brightfield microscopy (scale bar: 200 μM). Primary human hepatocyte donor cell health and functionality evaluated in the Liver MPS with (D) albumin production, (E) urea production, (F) CYP3A4 activity and (G), LDH a marker of cytotoxicity. LDH, lactate dehydrogenase.

2.4. Establishment of the primary Gut/Liver MPS

Liver microtissues were established by seeding PHHs in the liver compartment of the Dual-organ plate at day 9 and functionality evaluated as described in the section *Set-up of the Liver MPS*. The primary gut model was introduced into the gut compartment of the Dual-organ plate to begin coculture at day 13. To enable the coculture of the primary gut model and liver microtissues, 2 proprietary media were developed that share the same basal media but with distinct chemical supplements to maintain differentiation of the gut barrier tissue and metabolic functionality of the liver microtissues. Here, 325 μL of gut/liver apical medium (GAM; CN Bio Innovations) was added to the apical side of the gut compartment, and a total of 2600 μL of gut/liver circulation medium (GCM; CN Bio Innovations) was added to the basolateral side of the gut compartment (750 μL) and the liver compartment (1850 μL), which are fluidically connected under a flow rate of 1.0 $\mu\text{L/s}$ (Supplemental Table 1). During coculture, medium in the basolateral side of the gut compartment and liver compartment was recirculated under a flow rate of 0.5 $\mu\text{L/s}$ and 1 $\mu\text{L/s}$, respectively. The media described are buffered solutions with a pH of 7.7, measured by an electronic pH meter (Mettler Toledo).

2.5. Establishment of the Caco-2/Liver MPS

To establish the Caco-2/Liver MPS, Caco-2 cells were seeded at 5×10^4 viable cells on a 24-WP Transwell (6.5 mm diameter, 0.4 μm pore polyester membrane; Corning) in Caco-2 Growth Medium composed of Dulbecco's modified Eagle's medium (Thermo Fisher Scientific) supplemented with 1% penicillin-streptomycin (Merck), 10% fetal bovine serum (Thermo Fisher Scientific), 1% GlutaMAX (Thermo Fisher Scientific), and 1% Non-Essential Amino Acids solution (Thermo Fisher Scientific). Medium volumes were 250 μL (apical) and 750 μL (basal), changed every 2–3 days with TEER used to assess barrier integrity before addition to the Dual-organ

plate at 17 days postseeding. The corrected TEER was determined by subtracting the value from a Transwell without cells in Caco-2 Growth Medium from the test Transwell and multiplied by surface area. To establish the Caco-2/Liver MPS, 325 μL of Caco-2 Apical Medium (CAM) composed of Dulbecco's modified Eagle's medium supplemented with 1% penicillin-streptomycin, 1% GlutaMAX, 1% Non-Essential Amino Acids solution, and 1% Insulin–Transferrin–Selenium solution (Thermo Fisher Scientific) was added to the gut apical side of the gut compartment. GCM was added to the basolateral side of the gut compartment and the liver compartment at the same volume and circulated at the same flow rate as the primary Gut/Liver MPS.

2.6. Histology and imaging

Histological staining of gut barrier tissues cultured in 24-WP was performed on day 15 for the primary gut model and day 17 for the Caco-2 model. Transwells containing the barriers were fixed with 4% paraformaldehyde in 1 \times PBS for 15 minutes at room temperature, with the solution added to both the apical and basolateral sides. The membranes were then removed, stored in 70% ethanol, and embedded in paraffin wax. Tissue blocks were cut into 4- μm sections, dewaxed with xylene (Merck), rehydrated through ethanol gradients to 1 \times PBS, and stained with hematoxylin (Harris Hematoxylin; PFM Medical) and 1% alcian blue in 3% acetic acid (Merck). Brightfield images were captured using a light microscope (EVOS XL CORE Imaging System; Thermo Fisher Scientific).

2.7. Gene expression

Gene expression profiling involved collecting proliferative cells after 3 days in RGM and differentiated cells 5 days after switching to RMM. Cells were cultured as described in the *Primary gut model* section, but in a 12-well format. At the collection time point, cells

were rinsed once using $1\times$ PBS, followed by lysis in $500\ \mu\text{L}$ Transwell of RNA Lysis Buffer (Ambion RNAqueous kit; Invitrogen). The Ambion RNAqueous kit was employed for RNA isolation per the manufacturer's instructions. RNA yield was quantified using a Qubit. For cDNA synthesis, the iScript cDNA Synthesis Kit (Bio-Rad) was used. Gene expression was then measured via real-time PCR with the Biomark HD System and Fluidigm Dynamic Array IFCs at the UNC-Chapel Hill School of Medicine's Advanced Analytics Core Facility. TaqMan probes were purchased from Thermo Scientific (list of probes are provided in [Supplemental Table 2](#)). Relative gene expression was calculated ($2^{-\Delta\Delta C_t}$) by comparing each sample to the average value from the donor-matched proliferative cells and using 18S as the housekeeping gene.

2.8. RNA bulk sequencing

Gene expression profiling of gut barrier tissues cultured in 24-WP was performed on day 15 for the primary gut model and day 17 for the Caco-2 model. At the time of collection, cells were rinsed once with $1\times$ PBS and then collected in $300\ \mu\text{L}$ per Transwell of DNA/RNA shield (Zymo Research) and stored at $-80\ ^\circ\text{C}$. The Quick-RNA Microprep kit (Zymo Research) was used to isolate RNA based on the manufacturer's protocol. RNA concentration was quantified with a fluorometer (Qubit 4 Fluorometer; Thermo Fisher Scientific), and RNA bulk sequencing was performed by Azenta Life Sciences. A detailed description of the library preparation and analysis of raw data is provided in [Appendix A. Supplemental material](#).

2.9. Primary Gut/Liver MPS dosing with 7-hydroxycoumarin

7-Hydroxycoumarin (7-HC; Merck) was used to validate the absorption and metabolic functionality of the primary gut and PHH donors in coculture. This fluorescent compound is converted to nonfluorescent 7-HC glucuronide by glucuronidation. 7-HC (1 mM) was added to the apical side of the gut compartment in GAM in wells with both the primary gut model alone and the primary gut model in coculture with the liver microtissue, and a blank Transwell with no cells. Samples of media were collected at a volume of $50\ \mu\text{L}$ in the liver compartment at 0, 1, 3, 5, 24, and 48 hours, and signal intensity was measured using a fluorescence plate reader (excitation 400/emission 528, FLX800; BioTek).

2.10. MDZ case study

The experiment was designed to estimate in vitro PK parameters and determine individual organ contributions to metabolism using mechanistic modeling. This involved 3 conditions: (1) liver only, (2) gut only, and (3) a coculture of gut barrier and liver tissues in the Dual-organ plate. MDZ (1 mg/mL in methanol; Merck) was administered to simulate either oral or IV dosing. For oral dosing, MDZ was mixed into either GAM or CAM and added to the apical side of the gut compartment in wells containing the primary gut or Caco-2 model, respectively. For IV dosing, MDZ was mixed into GCM, which fluidically connects the basolateral side of the gut compartment to the liver compartment. Samples of media were collected at a volume of $50\ \mu\text{L}$ in the liver compartment and $5\ \mu\text{L}$ in the apical side of the gut compartment at 0, 1, 2, 4, 6, 24, 48, and 72 hours ([Supplemental Table 1](#)). Gut apical media samples were diluted in $45\ \mu\text{L}$ of either GAM or CAM, depending on the gut barrier tissue. The samples were stored at $-80\ ^\circ\text{C}$ and sent for analysis of compound concentration by ultra-high performance liquid chromatography-tandem mass spectrometry (Pharmidex) with chromatographic details reported in [Supplemental Table 3](#). The fraction unbound in media was determined by Rapid

Equilibrium Dialysis (Fischer Scientific) followed by ultra-high performance liquid chromatography-tandem mass spectrometry (Xenogenesis) with chromatography-tandem details reported in [Supplemental Table 4](#).

2.11. Model construction and fitting

To model the movement of MDZ and 1'-hydroxymidazolam through the Gut/Liver MPS, 4 compartmental ordinary differential equation models were constructed. These models included 4 elementary compartments: gut apical, gut basolateral, enterocytes, and liver. By combining these elementary compartments, models of varying complexities were created, ranging from 2 to 4 compartments in total. All compartments were considered homogeneous. For compartments that include cells, the concentration across the cellular membrane was assumed to be at equilibrium. Each model was fitted to the entire data set using the minimize function from the Python package Lmfit.^{18,19} A differential evolution algorithm with appropriate bounds was used to minimize the loss function

$$L = \sum_{i=1}^n (y_i - f(x_i))^2 \quad (1)$$

across the whole data set where y_i and $f(x_i)$ are the natural log-transformed values of the experimentally determined and model predicted values, respectively. After modeling the data with linear liver clearance, nonlinearity was identified in the rate of liver clearance and was confirmed in the analysis of the log-transformed data over time. In an attempt to adequately model liver clearance, nonlinear intrinsic liver clearance (CL_{int}) was implemented for select models

$$CL_{\text{int}} = \frac{V_{\text{max}}}{K_m + C(t)} \quad (2)$$

Where, V_{max} and K_m are the maximal rate of liver clearance and the Michaelis constant, respectively, and $C(t)$ is the drug concentration at time t .

2.12. Model selection

The fitted models were ranked according to the Akaike information criterion (AIC),²⁰ which ranks the model according to their residuals and applies a penalty to models with more parameters. A lower AIC indicates a better performing model. Following AIC ranking, the best performing model was selected for further analysis. For each model, the AIC was calculated as

$$AIC = 2k + n \log(\theta) \quad (3)$$

$$\theta = L/n \quad (4)$$

where n is the number of data points, k the number of parameters in the model, and L is the residual sum of squares from eq. 1.

2.13. Parameter estimations

A Markov Chain Monte Carlo algorithm was used to investigate the parameter space of the best performing model. A combination of the Lmfit¹⁸ and emcee²¹ Python packages were used to generate posterior distributions for each parameter. The starting values for the parameters were set to those obtained from the model fitting. Uniform distributions with the same bounds as in the parameter fitting were used as priors. The autocorrelation time, τ , was

calculated for each parameter, and the algorithm was run to ensure the number of samples was larger than 50 τ for each parameter to ensure statistically independent samples. A total of 20 walkers were used with a total chain length of 20,000. Using a burn-in period of 2000, the remaining 18,000 steps were used to construct the parameter posteriors. In the case of the nonlinear liver clearance, the $CL_{\text{int,liver}}$ (MDZ) posterior was estimated from the V_{max}/K_m ratio.

2.14. F_a , F_g , F_h , and F calculations

A prediction of bioavailability was determined from the model predicted parameters using the relationship

$$F = F_a \times F_g \times F_h \quad (5)$$

Where F_a , F_g , and F_h are the fraction absorbed, fraction escaping the gut, and the fraction escaping the liver, respectively. To estimate a mean, upper and lower bound for F_a , F_g , and F_h and F , the calculation for each of these constituent parts was repeated a total of 5000 times using parameters randomly drawn from the probability distributions resulting from the Bayesian inference analysis.

F_a estimation was performed as outlined by Yim et al, by first converting the model predicted value of P_{app} to P_{eff} , using a regression curve,²² followed by relating the effective permeability to drug permeability through the gut wall⁶

$$\log(P_{\text{eff}}) = 0.4926 \cdot \log(P_{\text{app}}) - 0.1454 \quad (6)$$

$$F_a = 1 - e^{-\frac{2 \cdot P_{\text{eff}} \cdot T_{\text{res}}}{R}} \quad (7)$$

Where T_{res} and R are the transit time (3 hours) and the radius of the small intestine (2 cm), respectively.

To calculate F_g , the model was simulated under 2 conditions: (1) with the $CL_{\text{int,gut}}$ as predicted by the parameter fittings and (2) by setting $CL_{\text{int,gut}} = 0$. A model area under the curve (AUC) was next calculated in the liver compartment for each of these simulated conditions. For the simulation of $CL_{\text{int,gut}} = 0$, this is the only change made to the model, and therefore, the only change that effects the model AUC. The calculation of F_g is made by taking the ratio of

$$F_g = \frac{\text{AUC}_{CL_{\text{int,gut}}}}{\text{AUC}_{CL_{\text{int,gut}}=0}} \quad (8)$$

For F_h , the parameter estimated $CL_{\text{int,liver}}$ was used to estimate the extraction ratio of MDZ from the liver using the well-stirred model. First, the in vivo CL_{int} was calculated by scaling the in vitro liver clearance

$$CL_{\text{int}} = \frac{CL_{\text{int,liver}} \cdot \text{SF} \cdot \text{HLW}}{n_{\text{liver cells}} \cdot fu_{\text{med}}} \quad (9)$$

where SF is the hepatocyte scaling factor (120 million hepatocyte cells/g liver), HLW is the average human liver weight (21.5 g liver/kg body weight), $n_{\text{liver cells}}$ is the number of liver cells seeded on the scaffold, and fu_{med} is the experimentally determined fraction unbound of MDZ in the media (Supplemental Table 5). The in vivo clearance was then used in the well-stirred model to estimate the in vivo hepatic clearance (CL_h), which was subsequently used to estimate the extraction ratio (E_h) followed by the fraction escaping the liver

$$CL_h = \frac{Q_h \cdot fu_b \cdot CL_{\text{int}}}{Q_h + fu_b \cdot CL_{\text{int}}} \quad (10)$$

$$E_h = \frac{CL_h}{Q_h} \quad (11)$$

$$F_h = 1 - E_h \quad (12)$$

where Q_h is the hepatic blood flow (20.7 mL/min/kg) and fu_b is the fraction unbound in blood (Supplemental Table 5).

2.15. Computational modeling

All mathematical modeling and calculations were performed using Visual Studio 2022 (Microsoft) and Python 3.11. The Python packages used in the computational work were numpy,²³ pandas,²⁴ scipy,²⁵ Lmfit,^{18,19} and emcee.²¹

3. Results

3.1. Functionality of the PHH donor in the Gut/Liver MPS

In this study, we connected PHHs with a primary gut barrier tissue to estimate the PK parameters of orally dosed compounds in vitro. A key feature of the Gut/Liver MPS is the circulation of cell culture medium, which serves 2 purposes: maintaining the functionality of PHHs in vitro for several weeks and linking the basolateral side of the gut barrier tissue with the liver microtissue to enable first-pass metabolism (Fig. 1, A and B). We first assessed the functionality of PHHs individually in the Liver MPS, before combining it with the primary gut barrier tissue. The Liver MPS has a recirculating liver compartment identical in volume, flow rate, and scaffold to the liver compartment in the Gut/Liver MPS (Fig. 1B). Over 14 days, functionality was demonstrated by 3D tissue formation (Fig. 1C), albumin production (Fig. 1D), urea production (Fig. 1E), CYP3A4 activity (Fig. 1F), and decreasing levels of lactate dehydrogenase, a marker of cell and tissue damage (Fig. 1G), consistent with previously published results.²⁶ The quantitative range of albumin (~30–60 $\mu\text{g/day}/10^6$ cells) and urea (~120–250 $\mu\text{g/day}/10^6$ cells), hallmarks of functionality of cultured hepatocytes, were comparable to that estimated in vivo for humans (>37 and >56 $\mu\text{g/day}/10^6$ cells for albumin and urea).²⁷ This provided confidence in the functionality of the PHH donor to be used in the Gut/Liver MPS.

3.2. Primary gut model characterization and donor functionality

The primary gut model was derived from the jejunum of a transplant-grade donor. The jejunum was selected as the model for the gut barrier because it is the intestinal region where most orally administered drugs are absorbed, due to a combination of high surface area and intrinsic epithelial characteristics.²⁸ Crypt-resident proliferating cells were initially plated at subconfluence onto Transwell inserts coated with a biomimetic scaffold and grown to confluence. Post-confluence, monolayers were differentiated into gut barrier tissues comprised of both absorptive and secretory lineages (Fig. 2A). Cellular proliferation and differentiation were assessed by gene expression on day 3 postplating (proliferative phase) and day 5 in RMM (differentiation phase). Across 3 human donors, differentiated cells in the primary gut model showed lower expression of proliferation genes and higher expression of differentiation genes compared with proliferative cells (Fig. 2B). Barrier formation was assessed using TEER. TEER values progressively increased from day 3 after switching to RMM until day 8, reaching over 500 $\Omega \cdot \text{cm}^2$ by day 5 when coculture assays were initiated (Fig. 2C). Increasing TEER values correspond

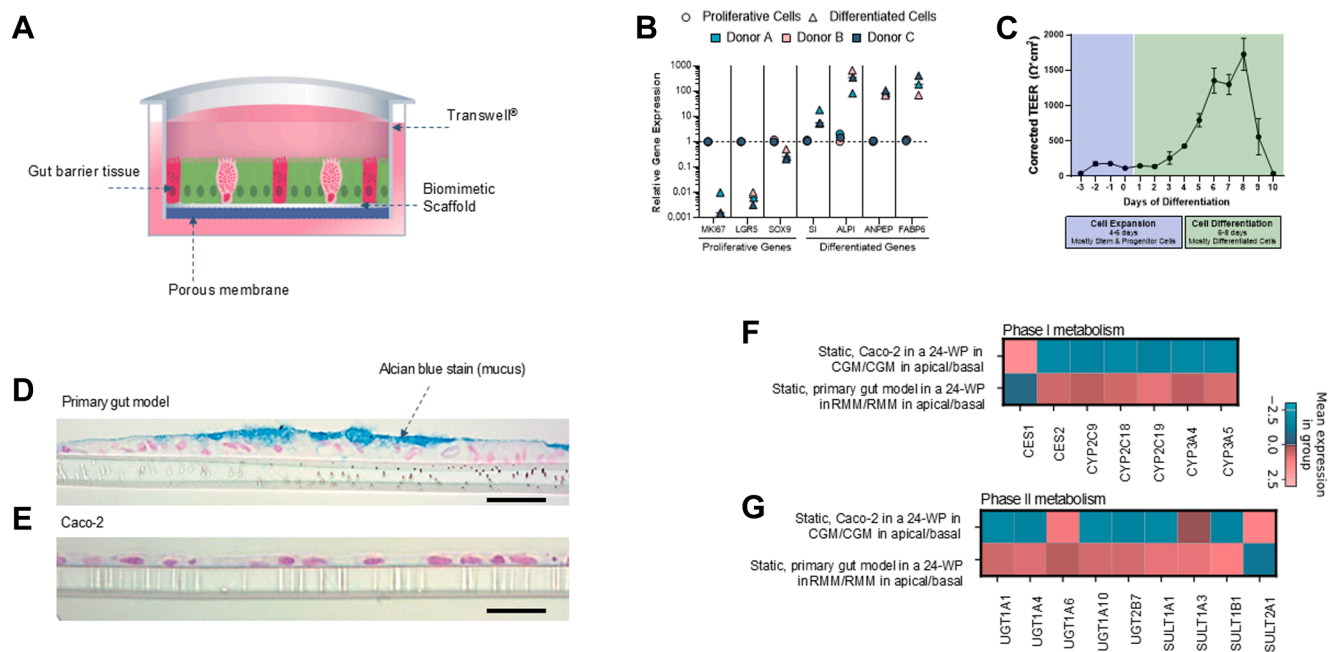


Fig. 2. Comparison of primary versus Caco-2 cell gut barrier tissue models. Schematic representation of (A) the primary gut model, RepliGut – Planar jejunum. (B) Gene expression of proliferative and differentiated cell genes in the primary gut model during proliferative and differentiation phases of cell culture relative to cells in the proliferative phase. Each data point represents average for an individual human donor, $n = 3$ donors and $n = 3$ replicates. (C) TEER curve of the primary gut model during cell expansion and differentiation phases. Data are represented as mean \pm SD; $n = 5$ technical replicates. Histology sections of the (D) primary gut barrier tissue at day 15 (or 5 days post-differentiation) and (E) Caco-2 barrier tissue at day 17 of culture in static conditions, stained with alcian blue and hematoxylin to visualize mucus and nuclei, respectively. Scale bar, 20 μ m. Comparison of gene expression of (F) Phase I and (G) Phase II metabolic enzyme genes with 3 replicates collected at day 15 in culture (5 days post-differentiation) for the primary gut model and day 17 for the Caco-2 model, cultured in static conditions in RMM and CGM respectively. CGM, Caco-2 growth medium; TEER, transepithelial electrical resistance.

to increasing enterocyte maturity; TEER decline after day 8 indicates the end of the culture's lifespan. Once fully differentiated, intestinal epithelial cells in culture have a finite lifespan of 3–10 days, which reflects their natural lifespan *in vivo*.²⁹ Differentiation into mucus-producing goblet cells, one of the postmitotic cell lineages, was confirmed by histology with a distinct and continuous layer of alcian blue, a marker of mucins (Fig. 2D). In contrast, Caco-2 cells, which are widely used in gut absorption studies, did not stain positive for alcian blue and have no distinct mucus layer (Fig. 2E).

Accurately estimating the PKs of orally dosed compounds depends on the functional levels of drug-metabolizing enzymes in the *in vitro* gut model. To evaluate the suitability of a primary gut model and assess the functionality of the donor used in this study, RNA bulk sequencing was used to measure the expression of genes indicative of phase I and phase II metabolism, compared with Caco-2 cells (Fig. 2, F and G). Most of the selected genes were significantly upregulated in the primary gut model compared with Caco-2 cells ($P < .05$), including CYP3A4, the main enzyme responsible for clearing compounds involved in gut first-pass metabolism (Fig. 2F). One exception was carboxylesterase 1, which was significantly upregulated in Caco-2 cells as compared with primary jejunum cells. This expression pattern in Caco-2 cells is inconsistent with the physiological expression pattern, as carboxylesterase 1 is predominantly expressed in the liver, not the small intestine.³⁰ In contrast, the primary gut model accurately reflects the human intestinal isoenzyme expression pattern with significant upregulation of carboxylesterase 2.

3.3. Establishing the primary Gut/Liver MPS for ADME studies

The primary Gut/Liver MPS was established by transferring Transwells with differentiated barrier tissues to the Dual-organ

plates on day 13, 4 days after PHH seeding. Once coculture was initiated, compounds were administered, with an assay window of up to 72 hours (Fig. 3A). One challenge with coculturing 2 or more primary tissues is maintaining the functionality of both tissue types. To address this, we designed a medium with specific chemical supplements to preserve the differentiation of the gut barrier tissue (GAM) and the metabolic functionality of the liver microtissues (GCM). This medium maintained hepatic functionality in coculture for 72 hours, as measured by CYP3A4 activity and albumin production, comparable to liver-only cultures in the Dual-organ plate (Fig. 3, B and C). The GAM/GCM media condition had no significant impact on primary gut culture TEER after 72 hours, as compared with standard culture conditions. Following incorporation of the primary gut culture into the Gut/Liver MPS, TEER levels plateaued. TEER values after 72 hours of cell culture continue to reflect a healthy tissue with strong barrier function (Fig. 3D). We validated the primary gut model and PHHs in coculture to demonstrate its utility in studying ADME processes. Using the compound 7-HC, which is metabolized through glucuronidation (Fig. 3E), we administered the compound to the apical side of the gut compartment for both primary gut-only and the primary gut in coculture with PHHs, sampling periodically from the liver compartment. Our results show functional 7-HC extraction by the primary gut model and the impact of adding PHHs, which reduces the AUC of the compound (Fig. 3F).

3.4. Pharmacokinetics of MDZ using the Gut/Liver MPS

We chose to evaluate the PKs of MDZ in the Gut/Liver MPS due to the well-established roles of these organs in its metabolism. MDZ, along with its main metabolite, 1'-hydroxymidazolam, is commonly used as a probe drug to evaluate CYP3A activity, the most abundant P450 subfamily expressed in the gut wall.^{8,31} To

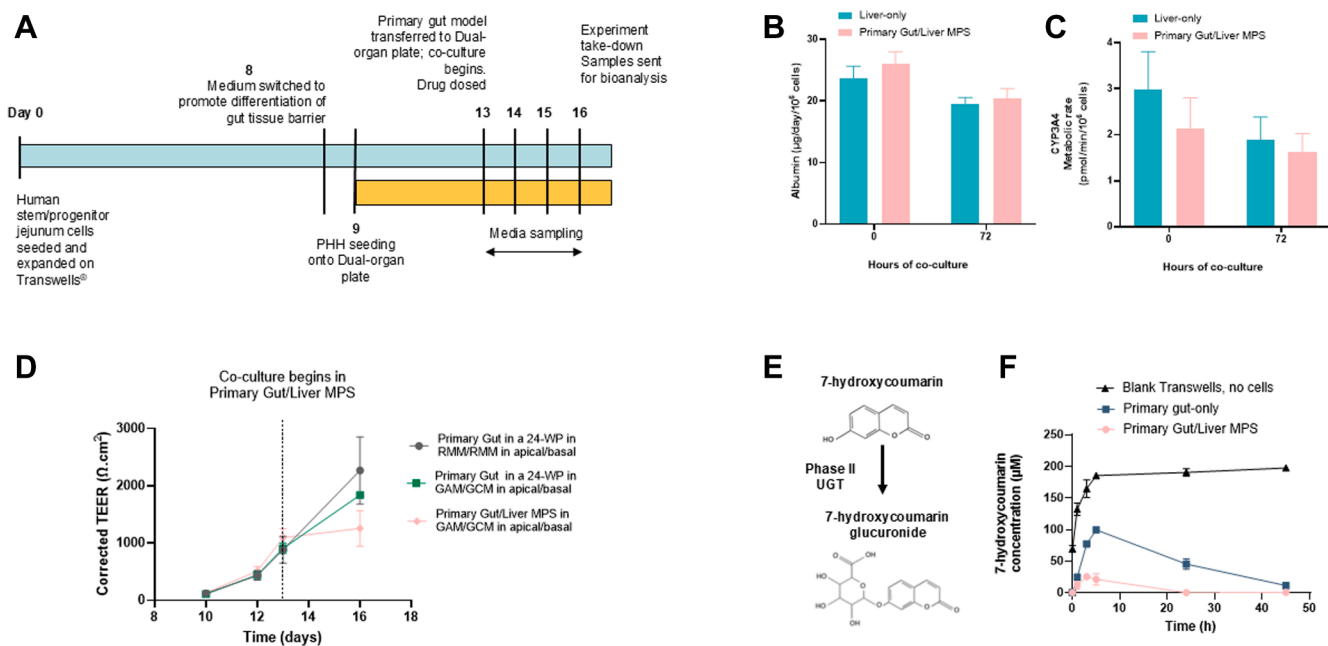


Fig. 3. Liver and gut functionality markers are maintained throughout the primary cell Gut/Liver coculture. (A) Experiment timeline to establish the primary Gut/Liver MPS. Markers of PHH functionality (B) albumin production and (C) CYP3A4 activity. (D) The barrier integrity of the primary gut model in the Gut/Liver MPS was assessed using TEER. (E) Validation of the primary gut model and PHHs in coculture to demonstrate its utility in studying ADME processes with the compound 7-HC. (F) 7-HC was administered to the apical side of the gut compartment for both primary gut alone and the primary gut in coculture with PHHs, sampling periodically from the liver compartment. Data are represented as mean \pm SD; $n = 3$ biological replicates. 7-HC, 7-hydroxycoumarin; ADME, absorption, distribution, metabolism, and excretion; PHH, primary human hepatocytes; TEER, transepithelial electrical resistance.

separate the contributions to metabolism by the gut and liver and enable model fittings in each organ, the experiment was conducted using gut-only, liver-only, and gut/liver setups. Gut-only and gut/liver experiments were run with both the primary gut model and the current standard cell line used in ADME studies, Caco-2, in order to directly assess the primary gut model for functional improvements.

For the liver-only condition, MDZ was administered directly to the interconnected liver and gut basolateral compartments, in the presence of an empty Transwell with no gut cells, to simulate an IV dose of 5 μ M. This concentration was lower than the oral doses used for the gut-only and gut/liver conditions (50 μ M) to achieve a constant total amount of drug in the system. The dilution occurs when the drug passes through the gut barrier tissue into the larger volume of the interconnected gut basolateral and liver compartments. In the liver-only experiment, MDZ concentration steadily decreased over time in the liver compartment, with <100 nM remaining at 72 hours (Fig. 4A). The concentration of 1'-hydroxymidazolam increased over time, peaking at 48 hours before decreasing, possibly due to further metabolism into its glucuronide derivative. To check for any unspecific hydrolysis or binding, MDZ was evaluated in the media without cells at the same concentration as the liver-only condition. There was no effect found, with 100% of MDZ remaining at 72 hours compared with the initial sampling at 0 hours.

In the gut-only experiment, MDZ concentration decreases in the apical side of the gut compartment as it crosses the cell barrier and steadily increases in the liver compartment, eventually reaching a plateau (Fig. 4B). Despite the higher initial concentration for the primary gut-only model, the AUC was higher for Caco-2 only, suggesting hydrolysis by the primary gut model. This was confirmed with the detection of 1'-hydroxymidazolam, which shows a steady increase in the apical side of the gut compartment and liver compartment, demonstrating functional CYP3A4 activity

by the primary gut model compared with no metabolism by Caco-2 cells.

In the gut/liver experiment, the MDZ profile in the apical side of the gut compartment is similar to the gut-only experiment. The liver compartment shows a steady increase in MDZ concentration until 24 hours, after which it decreases as MDZ is metabolized (Fig. 4C). The AUC in the primary Gut/Liver MPS was lower compared with Caco-2/Liver MPS, replicating the profile in the gut-only experiment, now with the presence of the liver micro-tissue. The profile of 1'-hydroxymidazolam in the apical side of the gut compartment for the primary Gut/Liver MPS confirms functional CYP3A4 activity by the primary gut model. However, the metabolite was also detected in the apical side of the gut compartment for Caco-2/Liver MPS, likely due to efflux from the basolateral side of the gut compartment driven by hepatic metabolism. In the liver compartment, 1'-hydroxymidazolam concentration peaks at 48 hours and drops at 72 hours, suggesting further metabolism into its glucuronide derivative. The AUC of 1'-hydroxymidazolam in the liver compartment was lower in the primary Gut/Liver MPS compared with Caco-2/Liver MPS, likely driven by differences in gut extraction levels.

3.5. Mechanistic model construction and parameter estimations

Mechanistic modeling of experimental data was conducted to estimate clearance and permeability parameters, using 4 models of increasing complexity to describe the transport and metabolism of compounds in the Gut/Liver MPS (Supplemental Fig. 1). These models, evaluated with AIC for ranking based on fit and complexity, varied in the number of compartments and assumptions. The simplest 2-compartment model included the gut apical and a combined gut basolateral and liver compartment, assuming rapid concentration equilibrium across enterocyte and hepatocyte membranes. In contrast, the 4-compartment model included the

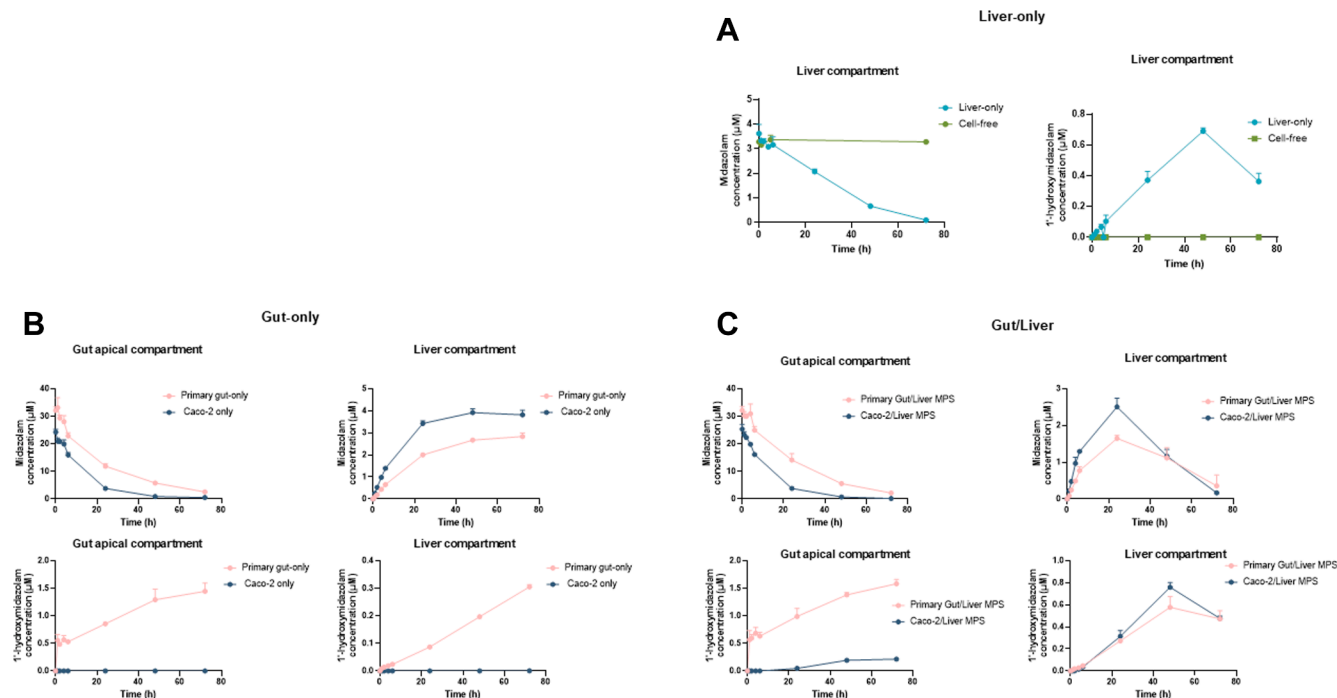


Fig. 4. Midazolam and 1'-hydroxymidazolam concentration over time in the primary Gut/Liver and Caco-2/Liver MPS. The concentration-time profiles for the (A) liver-only (B) gut-only and (C) gut/liver experiments. In liver-only and cell-free experiments, midazolam was mixed into the GCM to simulate an IV dose, with concentration-time profiles in the liver compartment only. The cell-free control was performed to quantify the rate of evaporation or nonspecific binding. Data are represented as mean \pm SD; $n = 3$ biological replicates. For the cell-free control, $n = 2$. GCM, gut/liver circulation medium.

gut apical, enterocytes, gut basolateral, and liver compartments, assuming rapid equilibrium only across hepatocyte membranes. AIC scores indicated better model fit with lower values; the 2-compartment model resulted in the lowest score. It was followed by the 3-compartment models, whereas the 4-compartment model ranked the poorest (Supplemental Table 6). Following the initial model selection, nonlinearity was identified in the rate of liver clearance, which was evident by the log-transformed concentration over time data from the liver-only experiment (Supplemental Fig. 2). To adequately model liver clearance, the 2-compartment model was fitted with Michaelis-Menten kinetics for MDZ liver clearance. This resulted in an improved AIC score resulting in the nonlinear 2-compartment model (Fig. 5A) being selected for further analysis and parameter distribution estimation (fitted model plotted with experimental data; Fig. 5, B–E, Supplemental Fig. 3, and Supplemental Fig. 4).

Using Bayesian inference to estimate the parameter posterior distributions, the best-fit parameters are presented in Table 1, whereas the full probability distributions for each parameter are detailed in Supplemental Fig. 5. These distributions are used downstream to determine estimates of bioavailability as shown in the workflow in Fig. 5F. Most parameters show well-defined probability spaces with clear minimums and maximums. The median values and 95% confidence intervals for each parameter were derived from their respective probability densities. However, parameters such as V_{max} and K_m show asymmetrical distributions with large right tails, indicating that these 2 parameters were less identifiable. V_{max} and K_m also showed a strong positive correlation with larger V_{max} values coinciding with larger K_m values. Although the range of V_{max} and K_m values is quite large, the overall clearance value, $CL_{int,liver}$ (MDZ), calculated from the V_{max}/K_m ratio, has a 95% confidence interval that is relatively narrow. Parameter estimates confirm experimental observations of clearance by the primary gut model (2.34 $\mu\text{L/h}$) with little to no measurable clearance detected by Caco-2 (0.0340 $\mu\text{L/h}$), although, this primary gut

metabolism remains a fraction of what is estimated by the liver microtissue (166 $\mu\text{L/h}$). Additionally, higher permeability across the gut barrier tissue was observed in Caco-2 compared with the primary gut model.

3.6. Bioavailability prediction

The bioavailability for MDZ was estimated by determining the F_a , F_g , and F_h , through model simulation of experimental data and by established scaling methods using model parameter estimates (Fig. 6A).^{32–35} For F_a , the predictions were estimated using the relationship between apparent permeability and drug permeability across the gut wall. The F_a for the primary Gut/Liver MPS and the Caco-2/Liver MPS was determined to be 0.93 and 0.98, respectively, which agrees with the human in vivo F_a of MDZ of 0.9^{32–34} (Fig. 6B). These values are consistent with the high permeability of MDZ, which was determined by our model estimates to be 31.3×10^{-3} cm/h for the primary Gut/Liver MPS and 74.6×10^{-3} cm/h for the Caco-2/Liver MPS. F_g was determined using the simulated AUC ratio of the oral dose, both with and without gut metabolism. It was estimated to be 0.79 for the primary Gut/Liver MPS and 1 for the Caco-2/Liver MPS. Although both values are higher than human estimates of F_g derived from indirect measurement using IV and oral clinical data,³² the primary Gut/Liver MPS demonstrates functional extraction of MDZ, compared with Caco-2 cells, which show no extraction (Fig. 6C). F_h was determined using the well-stirred model with the model-estimated value of $CL_{int,liver}$ (MDZ) and was found to be 0.64 and 0.66 for the primary Gut/Liver MPS and Caco-2/Liver MPS, respectively, which is in line with human in vivo data³² (Fig. 6D). Finally, F_a , F_g , and F_h were combined to estimate human oral bioavailability for MDZ. The model estimated it to be 0.47 for the primary Gut/Liver MPS and 0.65 for the Caco-2/Liver MPS, compared with 0.31 in humans, based on the mean weighted average from 36 studies³⁵ (Fig. 6E).

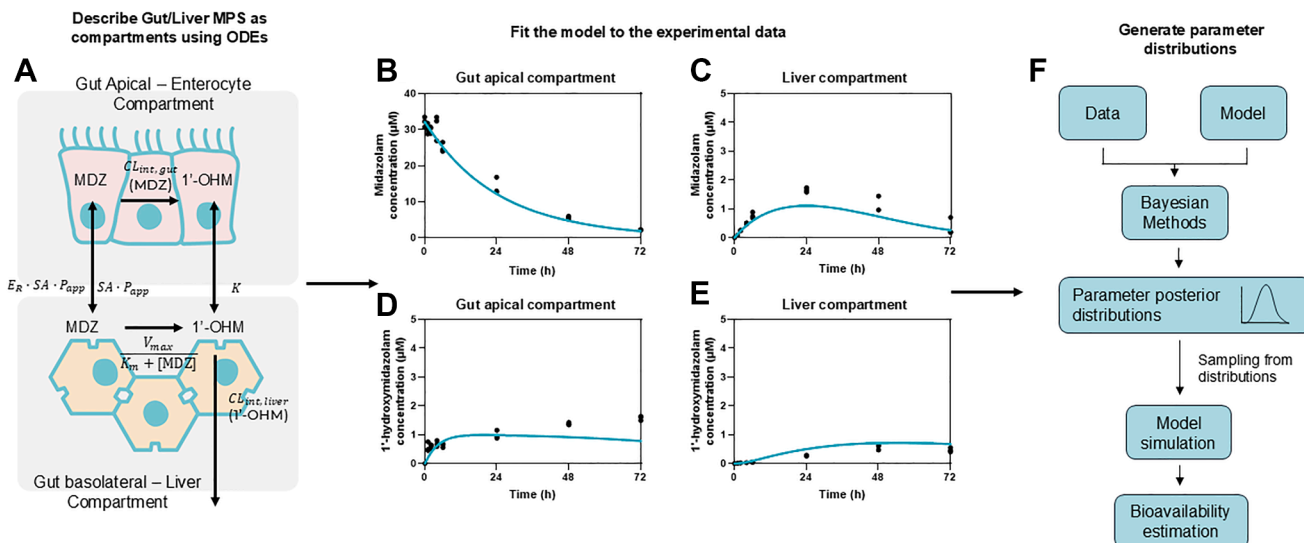


Fig. 5. Workflow for parameter estimations and posterior distributions leading to the prediction of human oral bioavailability. (A) Schematic representation of the movement of midazolam through the Gut/Liver MPS. The model schema shown outlines the structure of the best performing model and has 2 compartments, the gut apical-enterocyte compartment and the gut basolateral-liver compartment. The fitted model is plotted (B–E) with the experimental data for the primary gut/liver experiment. The model simulation is shown by the solid line and the experimentally determined values shown by the data points. The individual datapoints from triplicate experiments are shown here with only values above the Lower Limit of Quantification being plotted. The model is plotted for midazolam in the (B) apical and (C) liver compartment and for 1'-hydroxymidazolam in the (D) apical and (E) liver compartment. (F) After the initial fitting, the model and the data are used to estimate the posterior distributions of the parameters using Bayesian inference. The resulting parameters distributions are then used in Monte-Carlo simulations to estimate the bioavailability of midazolam as well as F_a , F_g , and F_h . MDZ, midazolam; MPS, microphysiological systems; OHM, 1'-hydroxymidazolam.

4. Discussion

In this study, we integrated mechanistic modeling with a Gut/Liver MPS to create a single platform that estimates human oral bioavailability and its components, F_a , F_g , and F_h , in vitro. This platform is based on an MPS that fluidically connects hepatocytes and gut barrier tissue, both derived from primary human sources to model gut absorption, gut metabolism, and hepatic metabolism.

We estimated F_a , F_g , and F_h from model simulations of experimental data and established scaling methods using model parameter estimates. For the components driven by the gut (F_a and F_g), our work builds upon and addresses the limitations of previous studies that cocultured PHHs with Caco-2 cells.^{16,17} We demonstrate that our primary gut model contains cells capable of transient proliferation and differentiation into multiple lineages and a distinct layer of mucus, both characteristics of the human intestinal lining.³⁶ Although the apparent permeability of MDZ through the primary gut barrier tissue was 2.5 times less than through the Caco-2 barrier, there was little difference in the predicted F_a , which

aligns with the human in vivo F_a of MDZ.^{32–34} The difference in predicted apparent permeability could be due to several factors, such as the influence of mucus on the apical side of the primary gut barrier tissue, the starting concentration, or the contribution of transporters. Transporter activity was indicated by the higher efflux ratio in the primary Gut/Liver MPS compared with the Caco-2/Liver MPS, with MDZ known to be a substrate of the P-glycoprotein transmembrane protein, which plays a role in drug efflux.³⁷ The prediction of F_a by the Gut/Liver MPS is likely to be most straightforward for compounds classified as Biopharmaceutics Classification System (BCS) class I, which have high permeability and high solubility, such as MDZ. For further assay validation, it is important to evaluate compounds across all BCS classes and to identify potential limitations, especially for challenging compounds with very low permeability. F_g is known to be the most challenging component of bioavailability to determine. Direct measurements of F_g in humans are rarely performed due to ethical reasons, with most data coming from either anhepatic patients during liver transplants or from indirect estimations based on in vitro and in vivo data.^{3,32,38}

Table 1
Table of parameter estimates for the 2-compartment model fitted to the primary Gut/Liver and Caco-2/Liver MPS data. The parameters estimated in the fitting are shown with the 95% confidence interval as determined from the Bayesian inference analysis. $CL_{int,liver}$ (MDZ) is the intrinsic clearance of midazolam by the liver and was calculated from the ratio V_{max}/K_m .

Parameter	Units	Primary Gut/Liver MPS		Caco-2/Liver MPS	
		Estimation	95% CI	Estimation	95% CI
V_{max}	pmol/h	318	174–1331	339	267–475
K_m	μM	1.91	0.580–11.99	2.14	1.45–3.47
$CL_{int,liver}$ (MDZ)	$\mu L/h$	166	107–304	158	136–185
$CL_{int,liver}$ (1'-OHM)	$\mu L/h$	34.6	7.6–70.2	15.8	4.4–28.1
$CL_{int,gut}$ (MDZ)	$\mu L/h$	2.34	2.07–2.65	0.0340	0.0215–0.0527
K	L/h	64.4	46.7–86.7	4.35	2.98–6.13
P_{app}	$\times 10^{-3}$ cm/h	31.3	26.9–36.9	74.7	70.5–79.5
E_R	Dimensionless	0.836	0.127–1.885	0.193	0.142–0.255
f_{met}	Dimensionless	0.235	0.151–0.351	0.217	0.193–0.243

OHM, 1'-hydroxymidazolam.

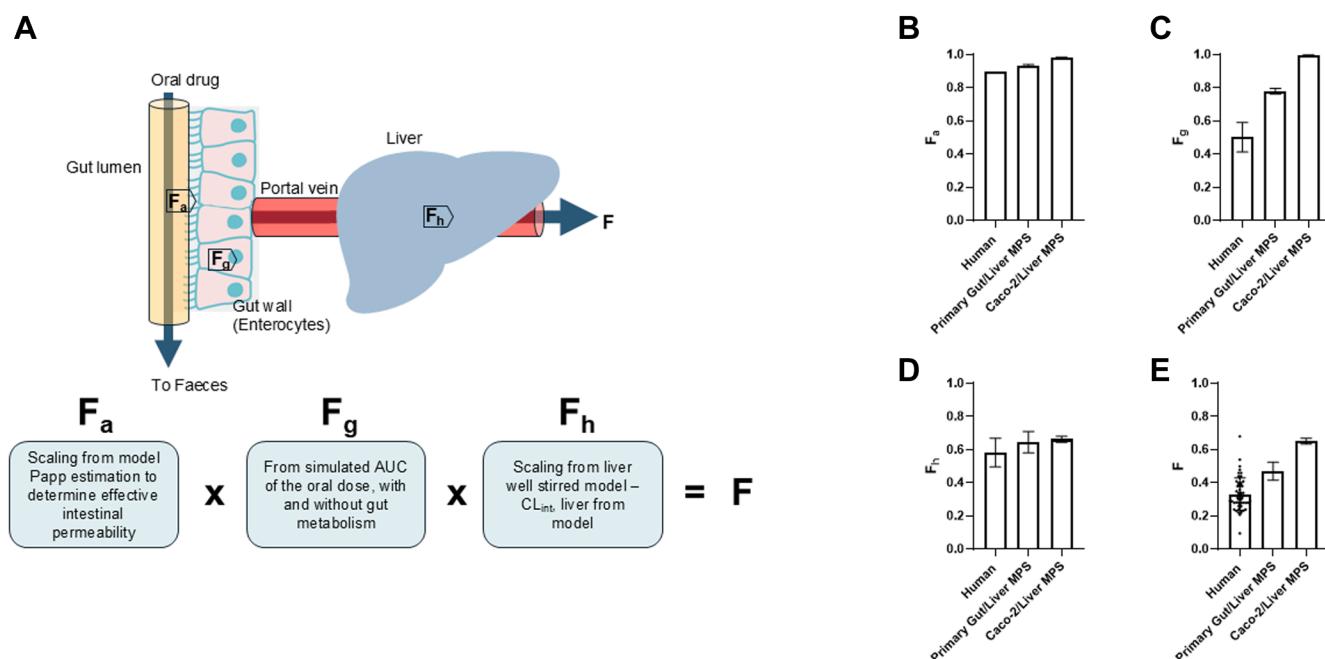


Fig. 6. Prediction of human oral bioavailability and its components F_a , F_g , and F_h of midazolam in the primary Gut/Liver MPS, compared to the Caco-2/Liver MPS and human estimations. (A) Diagrammatic representation of the components of bioavailability. F_a is shown as the fraction of drug that is absorbed into the enterocytes and does not pass all the way through the gastrointestinal tract. Enterocytes metabolize a fraction of the drug entering the gut wall, releasing the unmetabolized fraction of drug, F_g , into the portal vein which transports the drug to the liver. The incoming drug is metabolized as it passes through the liver and the fraction of drug that enters the systemic circulation in relation to the amount of drug that enters the liver is F_h . The bioavailability, F , is then calculated as the product of F_a , F_g , and F_h . Model simulations of experimental data and established scaling methods using model parameter estimates were used to generate MPS predictions of (B) F_a , (C) F_g , (D) F_h and (E) F for the primary Gut/Liver and Caco-2/Liver MPS compared to human estimations. The plotted graphs show the mean value with the error bars showing standard deviation. For F_a , the human estimation was taken from observations of midazolam absorption in clinical studies.^{32–34} For F_g and F_h estimates were taken from a study performing an indirect assessment from IV and oral clinical data with the reported mean and standard deviation shown in the plots.³² For F , the mean weighted average from 36 studies is shown, with each point the bioavailability value from a single study.³⁵ MPS, microphysiological systems.

Although scaling methods using minimal mathematical models such as Q_{gut} require only in vitro metabolic clearance and cell permeability data, this method relies on scaling parameters that are either difficult to identify or assumed, such as the number of enterocytes in the gastrointestinal tract, the fraction unbound of a compound in the gut, and the intestinal surface area.^{3,6,39} In this study, we measured the removal of the compound from the gut barrier using the relative AUC, with and without gut metabolism, similar to the approach used in gut CYP3A4 inhibition studies.⁴⁰ This mechanistic model enables complete inhibition of gut metabolism in silico while keeping all other parameters constant. This resulted in a F_g prediction of 0.79 in the primary Gut/Liver MPS. Although this is higher than the human predicted mean for F_g , it is an improvement compared with the Caco-2/Liver MPS, which had a value of 1.³²

Further improvements to the prediction of F_g could be achieved by lowering the oral dose to prevent CYP3A4 saturation of MDZ at high concentrations.⁴¹ Saturation is suspected from observations in the log-transformed data of MDZ in the liver-only experiment, which was dosed at a lower concentration. Administering a lower dose of 10 μ M, possible in the Gut/Liver MPS, may result in an increase in the $CL_{int,gut}$. Alternatively, F_g could be improved, and $CL_{int,gut}$ increased by increasing the number of enterocytes in the system; however, this involves a trade-off between surface area and apical volume, which is limited in Transwell-based gut models. These trade-offs are crucial in designing an MPS, where appropriate scaling enables more accurate in vitro to in vivo extrapolations. For multiorgan MPS, the challenge lies in scaling between organs such as tissue-to-tissue and tissue-to-volume ratios. There is no universally agreed upon approach. Common

methods include direct miniaturization, allometric scaling, or designing each organ to ensure functionality in a specific application context, followed by mechanistic modeling to obtain organ-specific parameters, as demonstrated in this study.^{15,42} When we compare the tissue-to-tissue clearance of the gut and liver, $CL_{int,liver}$ (MDZ) is approximately 1.4% of $CL_{int,liver}$ (MDZ). This aligns with human in vitro evidence, where the total mass of CYP3A in the entire small intestine, based on homogenates from isolated enterocytes, is estimated to be <1% of that in the liver.³

To determine the final component of bioavailability, F_h , we used the well-stirred model to scale $CL_{int,liver}$ (MDZ) for an in vivo prediction of liver clearance. This model has effectively scaled MPS-measured liver clearance, with prior studies adding in an evaporation constant to compensate for volume changes due to evaporation.⁴³ However, measuring evaporation rates is prone to inaccuracies due to challenges in collecting medium from microchannels and modeling frequent incubator openings in real-world experiments, which vary from lab to lab. To address this, we used cell-free control wells to measure changes in compound concentration from evaporation and nonspecific binding to materials in the MPS. Without cells, MDZ concentration remained constant over time, showing negligible nonspecific binding and evaporation. This approach allows direct measurement of compound concentration, and the rate of change can be incorporated into the estimation of compound liver clearance. MDZ clearance by the liver was modeled using Michaelis-Menten kinetics, which allows for modeling of nonlinearity, identified in the liver-only experiment. A decrease in the IV dose is expected to reduce nonlinear PKs of MDZ in the system, at concentrations closer to 1 μ M. Even with the nonlinear kinetics, the primary Gut/Liver MPS and Caco-2/Liver

MPS prediction of F_h were similar to that of human in vivo F_h measurements for MDZ.³²

The predicted oral bioavailability of MDZ of 0.47 using the primary Gut/Liver MPS aligns with the range observed in humans, which varies from 0.096 to 0.68, with a mean of 0.33.³⁵ This variability reflects the differing levels of hepatic and intestinal CYP3A activity in the human population,⁴⁴ which can be further investigated using different donor combinations or inclusion of pooled hepatocytes in the primary Gut/Liver MPS. Further applications of this model include investigating drug-drug interactions within the gut and liver, either individually or simultaneously. Additionally, it can be used to study nonlinear drug metabolism, as the Gut/Liver MPS can be dosed with varying compound concentrations to estimate metabolic saturation, activation, or inhibition. Parameter estimations from the primary Gut/Liver MPS can be integrated into physiologically based pharmacokinetic models to inform first-in-human dosing, leveraging more predictive in vitro human data. The US Food and Drug Administration recently cited this combined MPS and in silico modeling approach as a promising method to ensure more accurate predictions of human outcomes when evaluating the safety and PKs of drug compounds.⁴⁵ This signal of approval from the Food and Drug Administration represents a catalyst for rapid change; however, integration of these new approach methodologies into drug discovery workflows will take time. Chosen solutions must therefore be reproducible, commercially accessible, and proven to demonstrate advantages over traditional methods to expedite adoption. This study demonstrates the primary Gut/Liver MPS's potential to significantly enhance the drug discovery process via the generation of gut and liver specific parameters together with an estimation of human bioavailability all from a single in vitro platform. Furthermore, the platform offers the potential to modernize a broad range of additional ADME applications, future-proofing workflows in line with regulatory change. Looking ahead, future work should focus on validating the assay's reproducibility across a diverse range of drugs encompassing various metabolizing enzymes, transporters, and BCS classifications, and expanding the pool of cell donors to support broader regulatory acceptance and adoption.

In conclusion, we describe how a primary Gut/Liver MPS, combined with mechanistic modeling, can generate organ-specific PK parameters and estimate human oral bioavailability with its components: F_a , F_g , and F_h . We demonstrate the importance of using metabolically functional gut cells in combination with PHHs to estimate bioavailability for compounds subject to extensive first-pass metabolism. This work shows the potential of the primary Gut/Liver MPS, in conjunction with appropriate mechanistic modeling and scaling techniques, to be an invaluable tool for overcoming the limitations of animal models for estimating human ADME parameters such as bioavailability in vitro.

Abbreviations

ADME, absorption, distribution, metabolism, and excretion; AIC, Akaike information criterion; AUC, area under the curve; BCS, Biopharmaceutics Classification System; CAM, Caco-2 Apical Medium; $CL_{int,liver}$ (MDZ), intrinsic clearance of midazolam from the liver; $CL_{int,liver}$ (1'-OHM), intrinsic clearance of 1'-hydroxymidazolam from the liver; 3D, 3-dimensional; E_h , hepatic extraction ratio; E_R , Efflux ratio of midazolam across the enterocyte gut barrier; F_a , fraction absorbed; F_g , fraction escaping gut wall elimination; F_h , fraction escaping hepatic elimination; f_{met} , fraction of midazolam metabolism that results in 1'-hydroxymidazolam production; fu_b , fraction unbound of midazolam in blood; fu_{med} , fraction unbound of midazolam in media; GAM, gut/liver apical medium; GCM, gut/liver circulation medium; 7-HC, 7-

hydroxycoumarin; IV, intravenous; K, rate constant for 1'-hydroxymidazolam across the enterocyte gut barrier; K_m , Michaelis constant for midazolam clearance; MDZ, midazolam; MPS, microphysiological system; $n_{livercells}$, number of cells seeded on liver scaffold; P_{app} , apparent permeability of midazolam across the enterocyte gut barrier; PHH, primary human hepatocyte; PK, pharmacokinetic; Q_h , hepatic blood flow; R, radius of the small intestine; RGM, RepliGut Growth Medium; RMM, RepliGut Maturation Medium; SA, surface area of the Transwell; SF, hepatocyte scaling factor; TEER, transepithelial electrical resistance; T_{res} , transit time through the small intestine; V_{max} , maximal midazolam clearance rate; 24-WP, 24-well plate.

Financial support

This research received no specific grant from any funding agency in the public, commercial, or not-for-profit sectors.

Conflict of interest

Yassen Abbas reports a relationship with CN Bio Innovations Ltd that includes: employment. Yassen Abbas has patent pending to Assignee. Morné van Wyk reports a relationship with CN Bio Innovations Ltd that includes: employment. Hailey Sze reports a relationship with CN Bio Innovations Ltd that includes: employment. Hailey Sze has patent pending to Assignee. James Christophi reports a relationship with CN Bio Innovations Ltd that includes: employment. Ashley A. Spreen reports a relationship with Altis Biosystems that includes: employment. Ashley A. Spreen has patent pending to Assignee. R. Jarrett Bliton reports a relationship with Altis Biosystems that includes: employment. Elizabeth M. Boazak reports a relationship with Altis Biosystems that includes: employment. Elizabeth M. Boazak has patent pending to Assignee. Tomasz Kostrzewski reports a relationship with CN Bio Innovations Ltd that includes: employment. Tomasz Kostrzewski has patent pending to Assignee. A patent application has been submitted by CN Bio relating to this work and is currently pending.

Data availability

Differential gene expression data are deposited on figshare and available with the following <https://doi.org/10.6084/m9.figshare.29247311>. All other data are available from the corresponding author on reasonable request.

CRedit authorship contribution statement

Yassen Abbas: Conceptualization, Investigation, Formal analysis, Methodology, Project administration, Supervision, Validation, Visualization, Writing—original draft. **Morné Van Wyk:** Formal analysis, Methodology, Software, Visualization, Validation, Writing—original draft. **Hailey Sze:** Investigation, Methodology, Formal analysis, Validation. **James Christophi:** Investigation, Formal analysis. **Ashley A. Spreen:** Investigation, Formal analysis. **R. Jarrett Bliton:** Software, Visualization, Formal analysis. **Elizabeth M. Boazak:** Conceptualization, Formal analysis, Writing—review and editing. **Tomasz Kostrzewski:** Conceptualization, Supervision, Project administration, Writing—review and editing.

Declaration of AI and AI-assisted technologies in the writing process

During the preparation of this work the authors used Microsoft Copilot in order to improve the grammar and readability of certain sentences in the manuscript. After using this tool/service, the

author(s) reviewed and edited the content as needed and take(s) full responsibility for the content of the publication.

Supplemental material

This article has supplemental material available at dmd.aspetjournals.org.

References

- Price G, Patel DA. Drug Bioavailability. *xPharm: The Comprehensive Pharmacology Reference*. 2023;1–2. <https://doi.org/10.1016/B978-008055232-3.60035-2>
- O'Shea JP, Augustijns P, Brandl M, et al. Best practices in current models mimicking drug permeability in the gastrointestinal tract – an UNGAP review. *Eur J Pharm Sci*. 2022;170:106098. <https://doi.org/10.1016/j.ejps.2021.106098>
- Peters SA, Jones CR, Ungell AL, Hatley OJD. Predicting drug extraction in the human gut wall: assessing contributions from drug metabolizing enzymes and transporter proteins using preclinical models. *Clin Pharmacokinet*. 2016;55(6): 673–696. <https://doi.org/10.1007/s40262-015-0351-6>
- Jones CR, Hatley OJD, Ungell AL, Hilgendorf C, Peters SA, Rostami-Hodjegan A. Gut wall metabolism. Application of pre-clinical models for the prediction of human drug absorption and first-pass elimination. *AAPS J*. 2016;18(3): 589–604. <https://doi.org/10.1208/S12248-016-9889-Y>
- Musther H, Olivares-Morales A, Hatley OJD, Liu B, Hodjegan AR. Animal versus human oral drug bioavailability: do they correlate? *Eur J Pharm Sci*. 2014;57(100):280–291. <https://doi.org/10.1016/j.ejps.2013.08.018>
- Yim DS, Choi S, Bae SH. Predicting human pharmacokinetics from preclinical data: absorption. *Transl Clin Pharmacol*. 2020;28(3):126–135. <https://doi.org/10.12793/TCP.2020.28.E14>
- Yamada N, Negoro R, Watanabe K, Fujita T. Generation of Caco-2 cells with predictable metabolism by CYP3A4, UGT1A1 and CES using the PiTch system. *Drug Metab Pharmacokinet*. 2023;50:100497. <https://doi.org/10.1016/j.dmpk.2023.100497>
- Gertz M, Harrison A, Houston JB, Galetin A. Prediction of human intestinal first-pass metabolism of 25 CYP3A substrates from in vitro clearance and permeability data. *Drug Metab Dispos*. 2010;38(7):1147–1158. <https://doi.org/10.1124/DMD.110.032649>
- Davies M, Peramuhendige P, King L, et al. Evaluation of in vitro models for assessment of human intestinal metabolism in drug discovery. *Drug Metab Dispos*. 2020;48(11):1169–1182. <https://doi.org/10.1124/dmd.120.000111>
- Hatley OJD, Jones CR, Galetin A, Rostami-Hodjegan A. Quantifying gut wall metabolism: methodology matters. *Biopharm Drug Dispos*. 2017;38(2): 155–160. <https://doi.org/10.1002/BDD.2062>
- Di L, Obach RS. Addressing the challenges of low clearance in drug research. *AAPS J*. 2015;17(2):352–357. <https://doi.org/10.1208/S12248-014-9691-7>
- Wikswa JP. The relevance and potential roles of microphysiological systems in biology and medicine. *Exp Biol Med (Maywood)*. 2014;239(9):1061–1072. <https://doi.org/10.1177/1535370214542068>
- Roth A. Human microphysiological systems for drug development. *Science* (1979). 2021;373(6561):1304–1306. <https://doi.org/10.1126/SCIENCE.ABC3734>
- Fowler S, Chen WLK, Duignan DB, et al. Microphysiological systems for ADME-related applications: current status and recommendations for system development and characterization. *Lab Chip*. 2020;20(3):446–467. <https://doi.org/10.1039/C9LC00857H>
- Edington CD, Chen WLK, Geishecker E, et al. Interconnected microphysiological systems for quantitative biology and pharmacology studies. *Sci Rep*. 2018;8(1):4530. <https://doi.org/10.1038/s41598-018-22749-0>
- Tsamandouras N, Chen WLK, Edington CD, Stokes CL, Griffith LG, Cirit M. Integrated gut and liver microphysiological systems for quantitative in vitro pharmacokinetic studies. *AAPS J*. 2017;19(5):1499–1512. <https://doi.org/10.1208/S12248-017-0122-4>
- Milani N, Parrott N, Ortiz Franyutti D, et al. Application of a gut–liver-on-a-chip device and mechanistic modelling to the quantitative in vitro pharmacokinetic study of mycophenolate mofetil. *Lab Chip*. 2022;22(15):2853–2868. <https://doi.org/10.1039/D2LC00276K>
- Newville M, Stensitzki T, Allen DB, Rawlik M, Ingargiola A, Nelson A. *lmfit: non-linear least-square minimization and curve-fitting for python*. *Astrophysics Source Code Library*. Published online June 2016.
- Newville M, Otten R, Nelson A, et al. *lmfit/lmfit-py*: 1.3.2. Published online July 2024. <https://doi.org/10.5281/zenodo.12785036>
- Akaike H. A new look at the statistical model identification. *IEEE Trans Autom Contr*. 1974;19(6):716–723. <https://doi.org/10.1109/TAC.1974.1100705>
- Foreman-Mackey D, Hogg DW, Lang D, Goodman J. emcee: the MCMC Hammer. Preprint. Published online February 16, 2012. arXiv:1202.3665. <https://doi.org/10.1086/670067>
- Sun D, Lennernas H, Welage LS, et al. Comparison of human duodenum and Caco-2 gene expression profiles for 12,000 gene sequences tags and correlation with permeability of 26 drugs. *Pharm Res*. 2002;19(10):1400–1416. <https://doi.org/10.1023/a:1020483911355>
- Harris CR, Millman KJ, van der Walt SJ, et al. Array programming with NumPy. *Nature*. 2020;585(7825):357–362. <https://doi.org/10.1038/s41586-020-2649-2>
- McKinney W. Data Structures for Statistical Computing in Python. In: van der Walt Stefan, Millman Jarrod, eds. Proceedings of the 9th Python in Science Conference; 2010:56–61. <https://doi.org/10.25080/Majora-92bf1922-00a>
- Virtanen P, Gommers R, Oliphant TE, et al. SciPy 1.0: fundamental algorithms for scientific computing in Python. *Nat Methods*. 2020;17(3):261–272. <https://doi.org/10.1038/s41592-019-0686-2>
- Rubiano A, Indapurkar A, Yokosawa R, et al. Characterizing the reproducibility in using a liver microphysiological system for assaying drug toxicity, metabolism, and accumulation. *Clin Transl Sci*. 2021;14(3):1049–1061. <https://doi.org/10.1111/CTS.12969>
- Baudy AR, Otieno MA, Hewitt P, et al. Liver microphysiological systems development guidelines for safety risk assessment in the pharmaceutical industry. *Lab Chip*. 2020;20(2):215–225. <https://doi.org/10.1039/C9LC00768G>
- Azman M, Sabri AH, Anjani QK, Mustafa MF, Hamid KA. Intestinal absorption study: challenges and absorption enhancement strategies in improving oral drug delivery. *Pharmaceuticals (Basel)*. 2022;15(8):975. <https://doi.org/10.3390/PH15080975>
- Snippert HJ, van der Flier LG, Sato T, et al. Intestinal crypt homeostasis results from neutral competition between symmetrically dividing Lgr5 stem cells. *Cell*. 2010;143(1):134–144. <https://doi.org/10.1016/j.cell.2010.09.016>
- Imai T, Imoto M, Sakamoto H, Hashimoto M. Identification of esterases expressed in Caco-2 cells and effects of their hydrolyzing activity in predicting human intestinal absorption. *Drug Metab Dispos*. 2005;33(8):1185–1190. <https://doi.org/10.1124/DMD.105.004226>
- Kanazawa H, Okada A, Igarashi E, et al. Determination of midazolam and its metabolite as a probe for cytochrome P450 3A4 phenotype by liquid chromatography–mass spectrometry. *J Chromatogr A*. 2004;1031(1–2): 213–218. <https://doi.org/10.1016/j.chroma.2003.12.039>
- Galetin A, Gertz M, Houston JB. Potential role of intestinal first-pass metabolism in the prediction of drug–drug interactions. *Expert Opin Drug Metab Toxicol*. 2008;4(7):909–922. <https://doi.org/10.1517/17425255.4.7.909>
- Heizmann P, Eckert M, Ziegler W. Pharmacokinetics and bioavailability of midazolam in man. *Br J Clin Pharmacol*. 1983;16 Suppl 1(Suppl 1):43S–49S. <https://doi.org/10.1111/j.1365-2125.1983.tb02270.x>
- Smith MT, Eadie MJ, Brophy TOR. The pharmacokinetics of midazolam in man. *Eur J Clin Pharmacol*. 1981;19(4):271–278. <https://doi.org/10.1007/BF00562804>
- Johnson TN, Batchelor HK, Goelen J, Hornblow RD, Dinh J. Combining data on the bioavailability of midazolam and physiologically-based pharmacokinetic modeling to investigate intestinal CYP3A4 ontogeny. *CPT Pharmacometrics Syst Pharmacol*. 2024;13(9):1570–1581. <https://doi.org/10.1002/PSF4.13192>
- Elmentaite R, Kumasaka N, Roberts K, et al. Cells of the human intestinal tract mapped across space and time. *Nature*. 2021;597(7875):250–255. <https://doi.org/10.1038/s41586-021-03852-1>
- Tolle-Sander S, Rautio J, Wring S, Polli JW, Polli JE. Midazolam exhibits characteristics of a highly permeable P-glycoprotein substrate. *Pharm Res*. 2003;20(5):757–764. <https://doi.org/10.1023/A:1023433502647>
- Paine MF, Shen DD, Kunze KL, et al. First-pass metabolism of midazolam by the human intestine. *Clin Pharmacol Ther*. 1996;60(1):14–24. [https://doi.org/10.1016/S0009-9236\(96\)90162-9](https://doi.org/10.1016/S0009-9236(96)90162-9)
- Yang J, Jamei M, Yeo KR, Tucker GT, Rostami-Hodjegan A. Prediction of intestinal first-pass drug metabolism. *Curr Drug Metab*. 2007;8(7):676–684. <https://doi.org/10.2174/138920007782109733>
- Gertz M, Davis JD, Harrison A, Houston JB, Galetin A. Grapefruit juice–drug interaction studies as a method to assess the extent of intestinal availability: utility and limitations. *Curr Drug Metab*. 2008;9(8):785–795. <https://doi.org/10.2174/138920008786049276>
- Nguyen HQ, Kimoto E, Callegari E, Obach RS. Mechanistic modeling to predict midazolam metabolite exposure from in vitro data. *Drug Metab Dispos*. 2016;44(5):781–791. <https://doi.org/10.1124/DMD.115.068601>
- Maass C, Stokes CL, Griffith LG, Cirit M. Multi-functional scaling methodology for translational pharmacokinetic and pharmacodynamic applications using integrated microphysiological systems (MPS). *Integr Biol (Camb)*. 2017;9(4): 290–302. <https://doi.org/10.1039/C6IB00243A>
- Docci L, Milani N, Ramp T, et al. Exploration and application of a liver-on-a-chip device in combination with modelling and simulation for quantitative drug metabolism studies. *Lab Chip*. 2022;22(6):1187–1205. <https://doi.org/10.1039/D1LC01161H>
- Lamba JK, Lin YS, Schuetz EG, Thummel KE. Genetic contribution to variable human CYP3A-mediated metabolism. *Adv Drug Deliv Rev*. 2002;54(10): 1271–1294. [https://doi.org/10.1016/S0169-409X\(02\)00066-2](https://doi.org/10.1016/S0169-409X(02)00066-2)
- FDA. *Roadmap to Reducing Animal Testing in Preclinical Safety Studies*; 2025. <https://doi.org/10.1177/026119291804600501>